Note: there are errors in some equations which occured during type-setting. These are highlighted, and the correct equations are included at the end of this document

Supporting Information

Stengel et al. 10.1073/pnas.0910126107

SI Text

Methods. ***Thermodynamic analysis of HSP18.1 oligomerization.*** There are two reasonable methods for considering the relative stability of the oligomers, where the concentration of the ith oligomer is given by $[P_i]$, and the concentration of monomers forming $i$mers is given by $i[P_i]$ The 'step-wise' free energy method (ΔG_{ST}) is based on sequential equilibria between protein oligomers of the form $P_1 + P_{i-1} \rightleftharpoons P_i$, with the corresponding free energy for each oligomer given by $\Delta G_{\mathrm{ST},i} = -RT \ln \frac{[P_i]}{[P_{i-1}][P_1]}$.

Alternatively, we can consider the relationship between a protein oligomer with its constituent monomers according to the equilibria $iP_1 \rightleftharpoons P_i$ to allow us to directly compare the relative stabilities of all oligomers, with respect to the concentration of free monomers. The corresponding 'average free energy per monomer' is given by$\Delta G_{AV,i} = -RT \ln \frac{[P_i]}{[P_1]}$, which reveals the difference between a monomer in solution and its bound state. This quantity is entirely independent of the formation mechanism, relying solely on the equilibrium concentration of the oligomer of interest, and the concentration of free monomer.

The concentration of each oligomer can be expressed as a function of the equilibrium constants and the concentration of free monomer according to either $[P_i] = P_1 K_{AV,i}$ or $[P_i] = \Sigma_{k=1}^{i} K_{ST,k} [P_1]^i$, where $K_{AV,1} = K_{ST,1} = 1$. The two equilibrium constants are therefore related through: $K_{AV,i} = \Sigma_{k=1}^{i} K_{ST,k} P^{i-1}$.

In such a system it is important to distinguish between the total oligomer concentration, $\sum_{i=1}^{n} [P_i]$, and the total concentration of monomers in the system, $\sum_{i=1}^{n} i[P_i]$. While the former varies with temperature-induced changes in the equilibrium size distribution, the latter does not and can be defined as $\sum_{i=1}^{n} i[P_i] = \sum_{i=1}^{n} iK_{AV,i}[P_1] = \Sigma_{i=1^i}^{n} \Sigma_{k=1}^{i} K_{ST,k} [P_1]^i$. From a complete set of equilibrium constants $[P_i]$ and hence the concentration of subunits partitioned into this oligomeric state $i[P_i]$ can be determined.

By plotting ΔG versus T we obtained ΔH and ΔS values for both the stepwise and average quantities. In the case of data presented here, the reduced χ^2 values $\chi^2/(N\text{-}p)$, where N is the number of data points, and p is the number of parameters, and $\chi^2 = \sum_{i}^{N} \frac{(\Delta G_i^{\exp} - \Delta G_i^{\mathrm{calc}})^2}{\sigma \Sigma_i^2}$ were determined to be in the range 1–1.5 when fitting to the linear model of $\Delta G = \Delta H - T\Delta S$.

We compared this to a more complex model $\Delta G = \Delta H^0 + \Delta C_P (T - T_0) - T(\Delta S^0 + \Delta C_P ln[T_0/T])$, where T_0 is a reference temperature, ΔH^0 and ΔS^0 are the enthalpy and entropy changes at this temperature, and ΔC_P is the change in heat capacity. An F-test between the fits to these models gave p values between 0.06 and 0.25 indicating that our measurements do not detect significant variation in heat capacity over the temperature range studied.

1. Benesch JLP, Aquilina JA, Ruotolo BT, Sobott F, Robinson CV (2006) Tandem mass spectrometry reveals the quaternary organization of macromolecular assemblies. *Chem Biol* 13:597–605.
2. Benesch JLP, Sobott F, Robinson CV (2003) Thermal dissociation of multimeric protein complexes by using nanoelectrospray mass spectrometry. *Anal Chem* 75:2208–2214.
3. Heck AJR, van den Heuvel RHH (2004) Investigation of intact protein complexes by mass spectrometry. *Mass Spectrom Rev* 23:368–389.
4. Kaltashov IA, Mohimen A (2005) Estimates of protein surface areas in solution by electrospray ionization mass spectrometry. *Anal Chem* 77:5370–5379.
5. de la Mora JF (2000) Electrospray ionization of large multiply charged species proceeds via Dole's charged residue mechanism. *Anal Chim Acta* 406:93–104.
6. Benesch JLP (2009) Collisional activation of protein complexes: Picking up the pieces. *J Am Soc Mass Spectrom* 20:341–348.
7. McKay AR, Ruotolo BT, Ilag LL, Robinson CV (2006) Mass measurements of increased accuracy resolve heterogeneous populations of intact ribosomes. *J Am Chem Soc* 128:11433–11442.

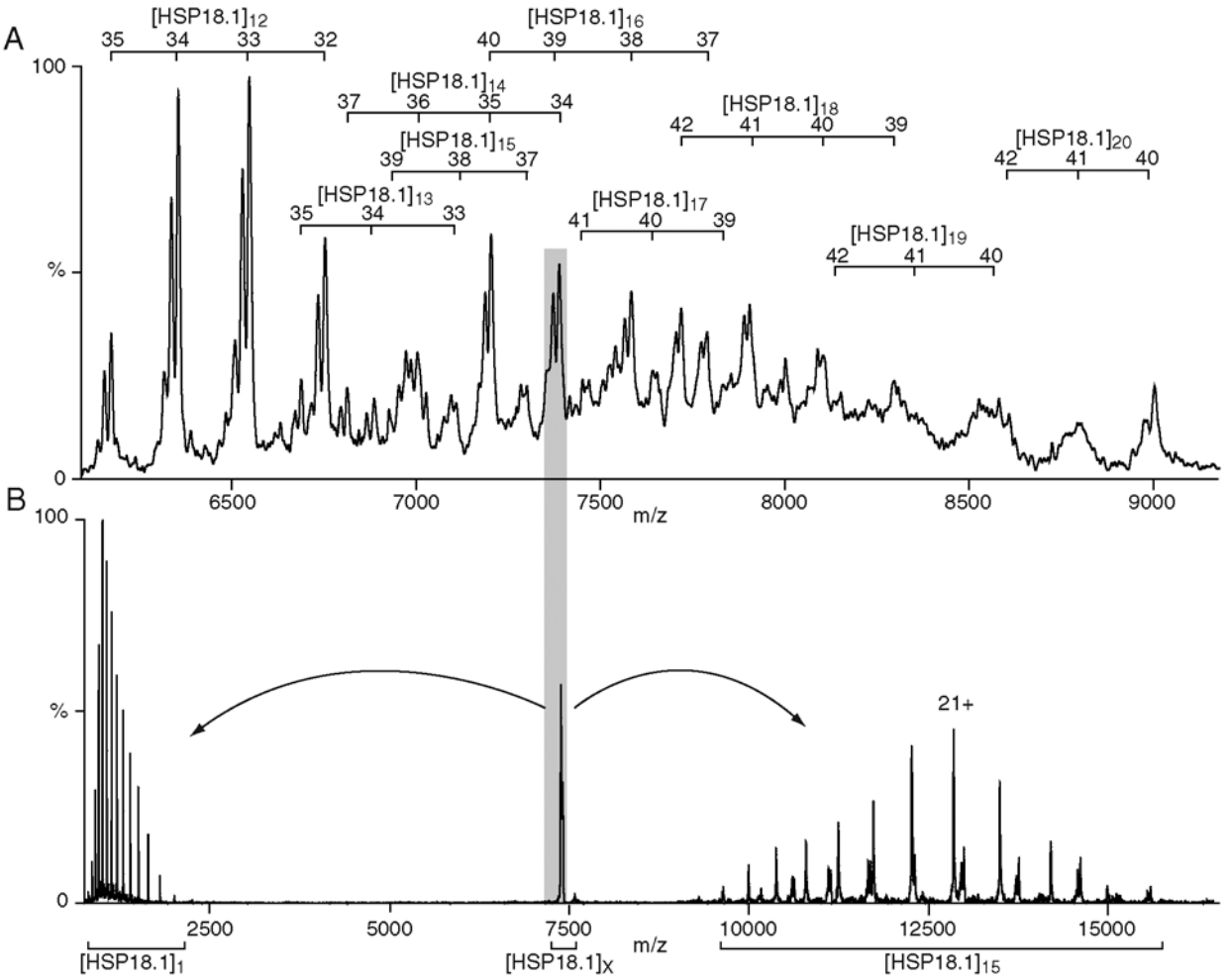

Fig. S1. Identification of higher-order oligomers of HSP18.1. At elevated temperatures HSP18.1 forms a range of species at higher *m/z* than the native dodecamers. To identify the various oligomers we used a combination of the observed *m/z* values (*A*) and tandem-MS experiments. In these tandem-MS experiments we isolated the peak of interest in the quadrupole analyzer of the Q-ToF mass spectrometer, and removed highly charged monomers from the oligomers by collision induced dissociation (1). For example, after isolation and dissociation of the species comprising the peak at 7, 380 *m/z* (*B*), we observed monomer at low *m/z*, and signal at high *m/z* corresponding primarily to a species of 269,775 Da, consistent with $[HSP18.1]_{15}$. As this species must arise from one having been stripped of a single monomer, the original oligomer corresponds to a $[HSP18.1]_{16}$. A minor amount of $[HSP18.1]_{13}$, hence from $[HSP18.1]_{14}$, is also observed. This process was then repeated for different peaks in the MS spectrum, thereby allowing us to identify all the oligomers which comprise the polydisperse ensemble of HSP18.1 at elevated temperature. Relative abundances were calculated from the peak heights in the MS spectrum, taking into account the contributions from the individual oligomers to the different peaks in the spectrum.

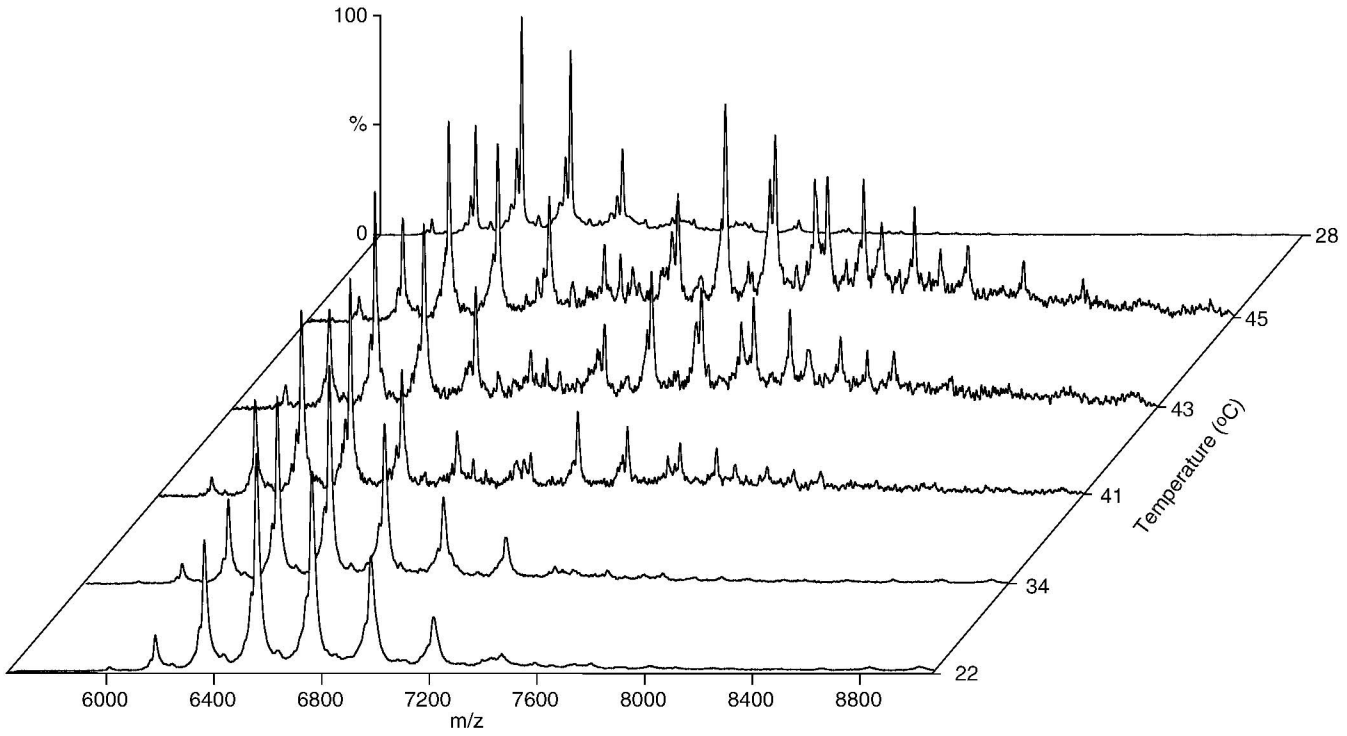

Fig. S2. Reversibility of changes in HSP18.1 oligomerization. To assess the reversibility of the thermally regulated changes in oligomerization of HSP18.1 we raised the temperature of the solution from 22 °C to 45 °C, and cooled it back down to 28 °C, while monitoring it continuously in real time using a customized nanoelectrospray probe (2). As the temperature increases the relative amount of dodecamer decreases, and concomitantly higher-order oligomers are formed. As the temperature of the 45 °C solution is reduced this shift is reversed, such that at 28 °C the dodecamer again dominates the spectrum. This cooling process took approximately 15 min. This demonstrates that the thermo-dynamically controlled changes in oligomerization are rapidly reversible. Data are normalized such that the dodecamer remains at 100%.

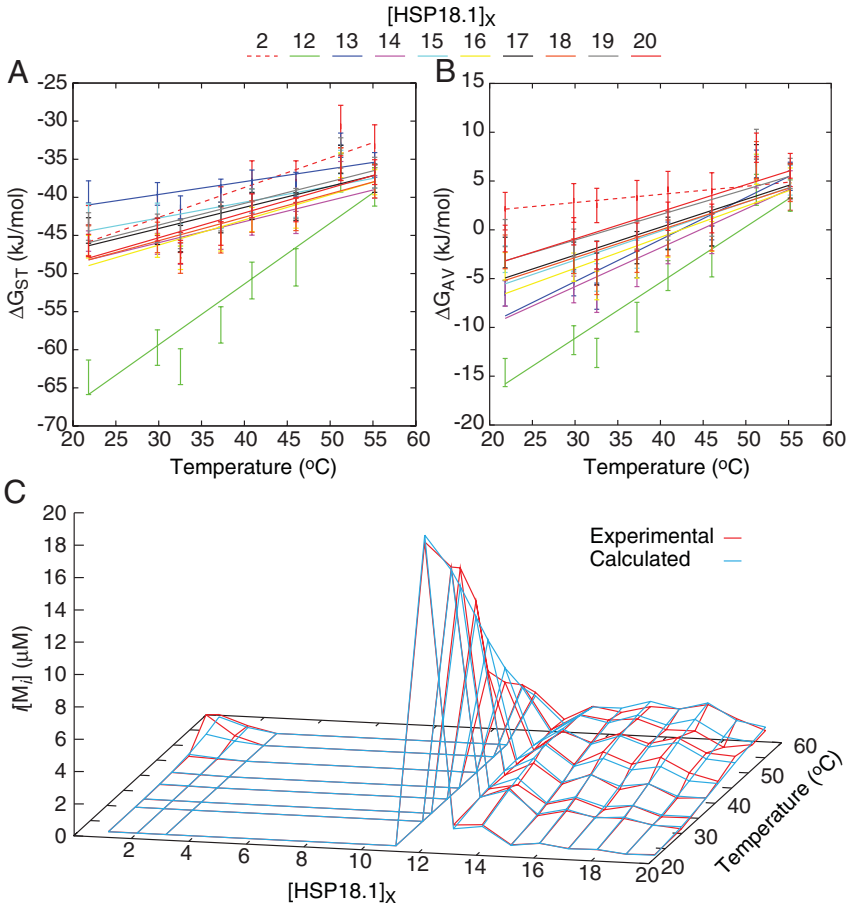

Fig. S3. (*A*) Thermodynamic analyses of the oligomers. Stepwise (*A*), and average (*B*), free energies were determined and analyzed according to $\Delta G = \Delta H - T\Delta S$ for the different oligomers populated by HSP18.1 at different temperatures (Fig. 1). In the case of the 12mer, as the concentration of oligomers of size between 3 and 11 was too low to be detected, the calculated ΔG_{ST} is defined through the equilibrium constant $K_{ST,12} = \frac{[M_{12}]}{[M_2][M_1]}$. The ΔH and ΔS values extracted in this way can be used to back calculate a population distribution at an arbitrary temperature. These back-calculated free energy distributions (shown here for ΔG_{AV}) were found to be in excellent agreement with that measured experimentally (*C*), confirming that the data can be well explained by considering the relative thermal stabilities of the individual oligomers. Although the dodecamer undergoes a large change in relative concentration over the temperature range studied, there is no evidence to suggest that the variation in size distribution is due to the formation of structurally distinct 'activated' complexes that radically alter the relative stabilities of the various complexes.

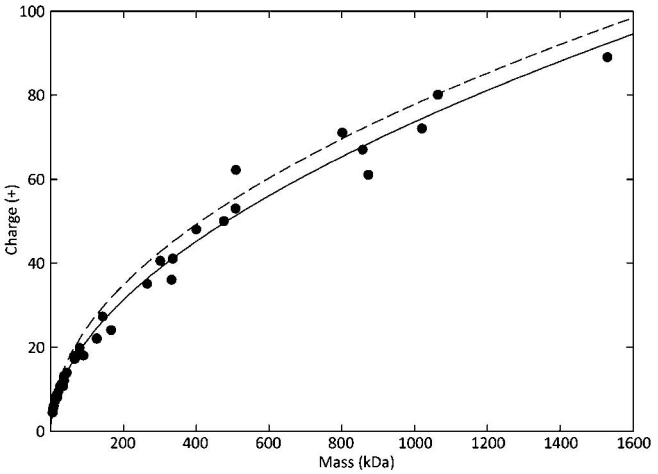

Fig. S4. Determination of the average mass of complexes. To determine a relationship for average m/z and average mass of the sHSP:client complexes we used two published data sets of charge state versus mass for a range of proteins and protein complexes (3, 4). Overlaid is a theoretical prediction of the maximum charge state (dashed line), derived from the Rayleigh limit for droplet fission, of $Z_{MAX} = 0.0778\sqrt{M}$ (5). From the experimental data we can obtain a line of best fit (*Solid Line*) for the data with a relationship for the average charge state: $Z_{AV} = 0.0467M^{0.5330}$. Therefore, by letting the *m/z* value of a peak in the mass spectrum be given by *T*, and with the simplification that the mass of the charge-giving protons is insignificant compared to the mass of the protein complexes: $T_{AV} = 21.4133M^{0.4670}$ and therefore: $M_{AV} = 0.0014O(T_{AV}^{2.1413}$. Based on these relationship between charge and mass we would expect a hypothetical $[HSP18.1]_{12}$ $[Luc]_1$ complex (276.7 kDa) to be centred on the 37+ charge state, with the principal five charge states therefore located between 7,094 and 7,905 *m/z* (39+ to 35 +). To calculate M_{AV} for the sHSP:client complexes, the broad area of signal corresponding to complexes was integrated, and T_{AV} was taken to be the weighted median *m/z* value (Fig. 2*B*).

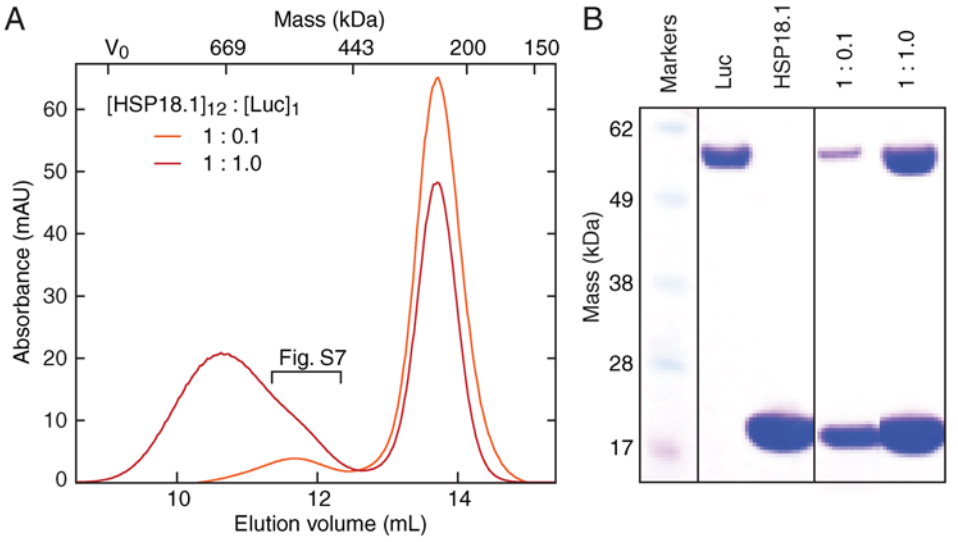

Fig. S5. SEC and SDS-PAGE of HSP18.1:Luc complexes. We formed complexes between HSP18.1 and Luc by incubating them at 42 °C for 10 min, at two different ratios, and analyzed them by means of SEC (*A*). At a 1:1 ratio (HSP18.1 dodecamer to Luc monomer), a broad peak centered on 10.5 mL, a fraction of which was used for MS analysis (Fig. S8), and a narrower peak at 13.7 mL were observed. SDS-PAGE, using pre-cut gels and the SeeBlue Plus 2 marker (both Invitrogen), of these peaks (*B*), show the former to contain both HSP18.1 and Luc, and the latter solely sHSP. Increasing the ratio of HSP18.1 to Luc results in a narrower complex peak and shifts it to longer elution times, implying a narrower distribution of lower average mass likely more amenable to MS analysis.

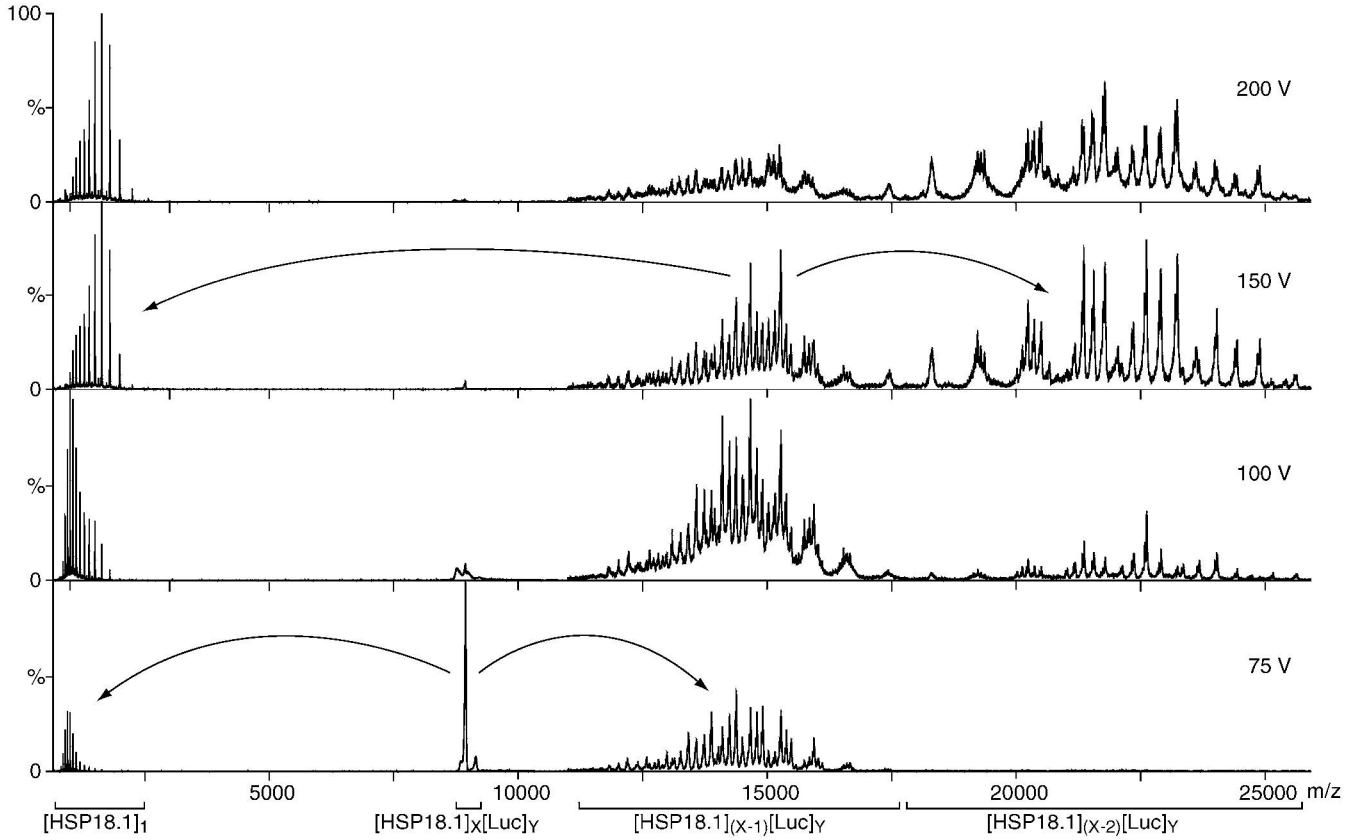

Fig. S6. Tandem-MS of HSP18.1:Luc complexes. The general mechanism of dissociation of protein complexes upon collisional activation is the loss of highly charged monomers from the parent oligomers (6). Moreover, multiple subunits can be removed, in a sequential manner, depending on the amount of activation (1). Performing tandem-MS of the peak at 8,950 *m/z*, as in Fig. 3, results in monomers at low *m/z*, and two distinct regions of signal at high *m/z,* centered at approximately 14,000 *m/z*, and approximately 22,000 *m/z*, respectively. At an acceleration voltage into the collision cell of 75 V only the former is populated. As the voltage is increased the latter region becomes progressively more dominant, such that at 200 V most of the signal resides therein. This shows that these regions therefore correspond to oligomers stripped of one and two monomers, respectively.

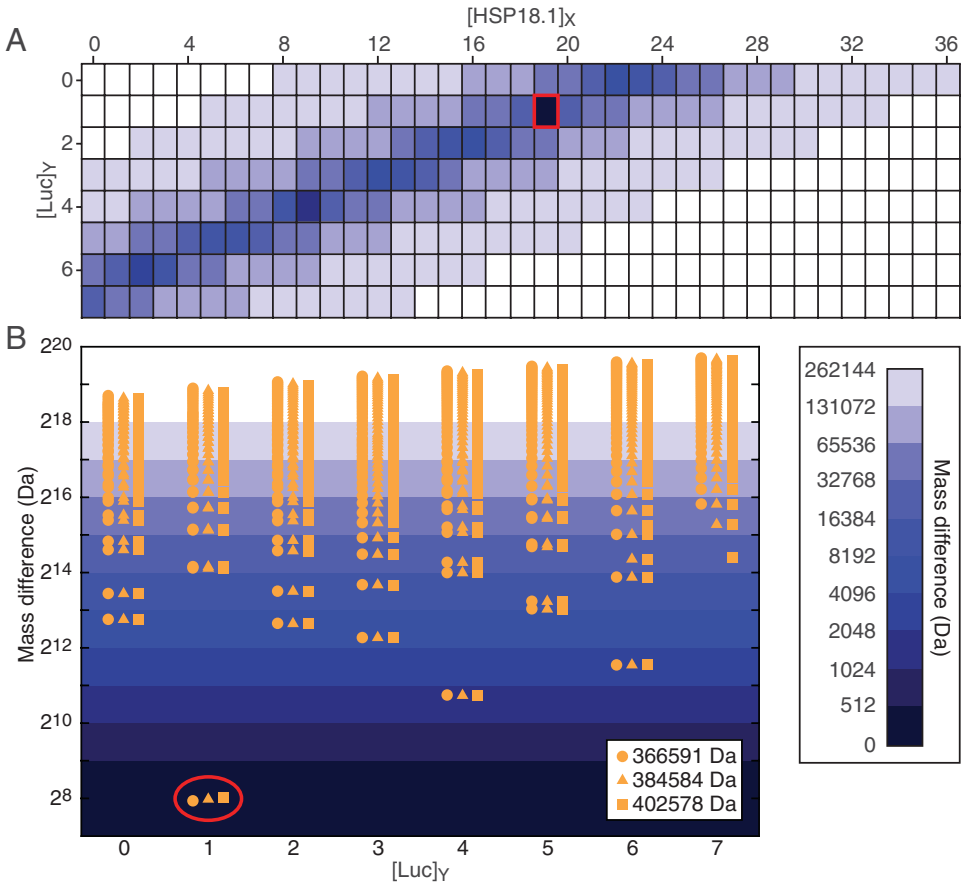

Fig. S7. Assignment of HSP18.1:Luc complexes. To assign the masses for complexes we measured in our tandem-MS spectra to particular combinations of HSP18.1 and Luc we constructed a matrix of theoretical masses based on the sequences of the individual proteins. Each measured mass was then compared to all possible combinations, and that with the lowest difference was taken to be the correct assignment. For example, from the spectrum shown in Fig. 3B, we obtained a mass from a charge state series of 402,578 Da. Comparing this with our theoretical matrix results in one possible combination, $[HSP18.1]_{19}[Luc]_1$, of much better correspondence than all others (*A*). The same procedure for other masses obtained from Fig. 3*B*, 366,591 Da and 384,584 Da, results in similarly unambiguous assignment (*B*). Common to all spectra of protein assemblies, a small discrepancy between measured and theoretical masses remains, due to the presence of residual solvent molecules and buffer ions (7).

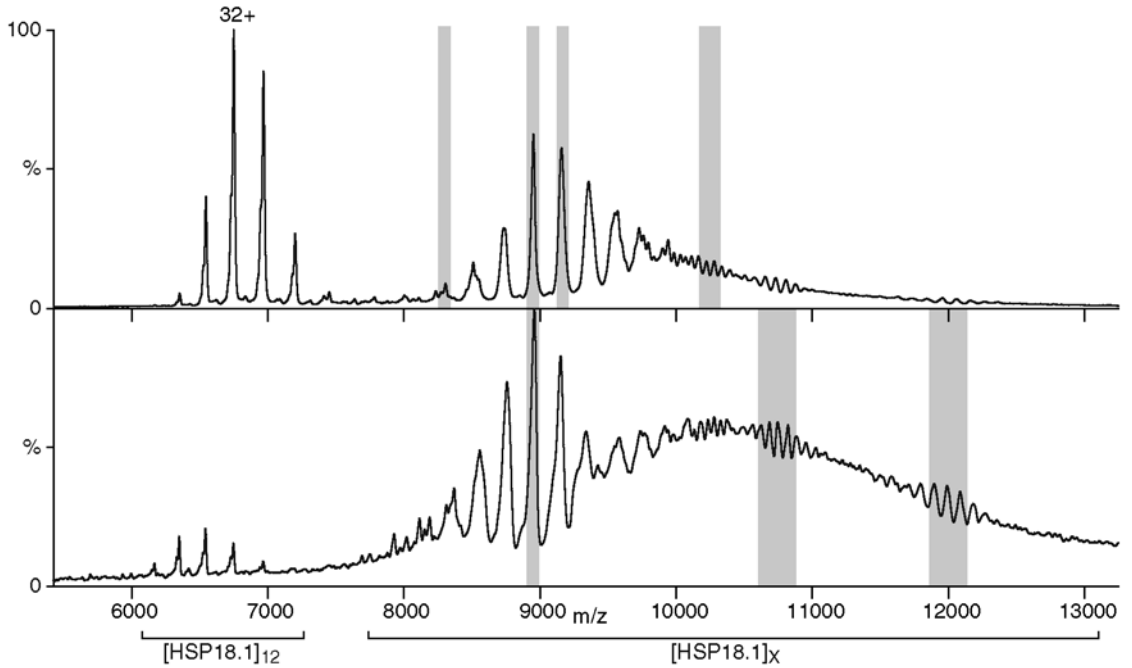

Fig. S8. Complexes formed at different ratios of HSP18.1 and Luc. We selected a number of regions of the MS spectra obtained for the complexes for tandem-MS interrogation. For a 1:0.1 ratio, upper panel, four separate isolations were performed and combined to enable a reconstruction of the overall distribution. For the 11.5–12.3 mL fraction, from incubation at a 1:1 ratio (*Lower*, Fig. S4), additional isolations up to approximately 12,000 *m/z* were performed.

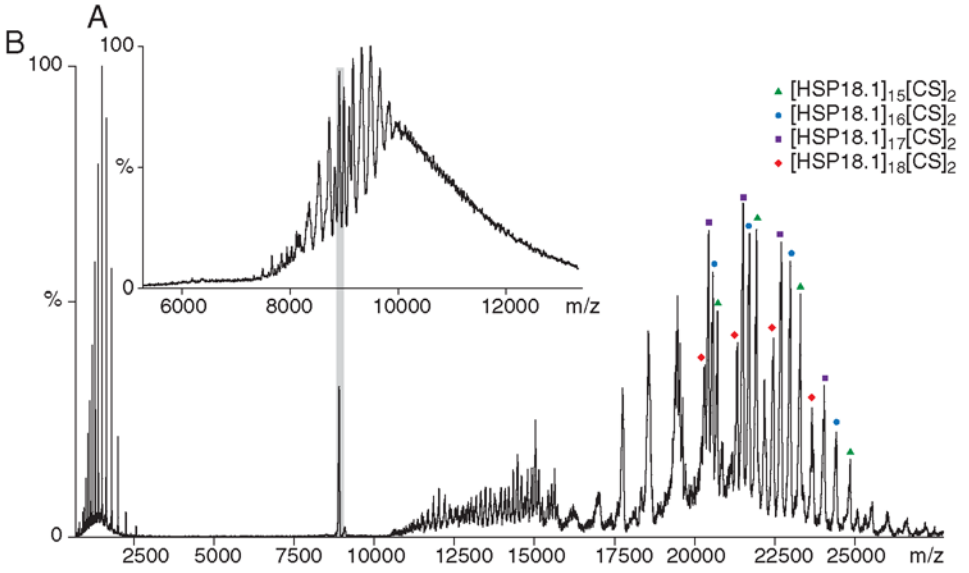

Fig. S9. Characterization of complexes between HSP18.1 and citrate synthase. Complexes were formed between HSP18.1 and citrate synthase (Sigma, Cat C3260-200UN) by incubation at a 1:0.25 molar ratio (dodecamer:dimer) at 45 °C for 60 min. A nES mass spectrum of the resultant complexes shows a broad area of signal from 7,000 to 14,000 *m/z*, consistent with a polydisperse ensemble of species (*A*) This mirrors what we observed with luciferase as client (Fig. 2*A*, Fig. 3*A*, Fig. S10). Selection and dissociation of the complexes at 8,900 *m/z* (*B*), allows the identification of different stoichiometries. In this spectrum we are able to unambiguously identify doubly stripped oligomers comprised of two citrate synthase subunits bound to between 15 and 18 subunits of HSP18.1. These experiments demonstrate that the polydisperse nature of client binding to HSP18.1 is not limited to Luc, but rather appears a general feature of this sHSP's chaperone function.

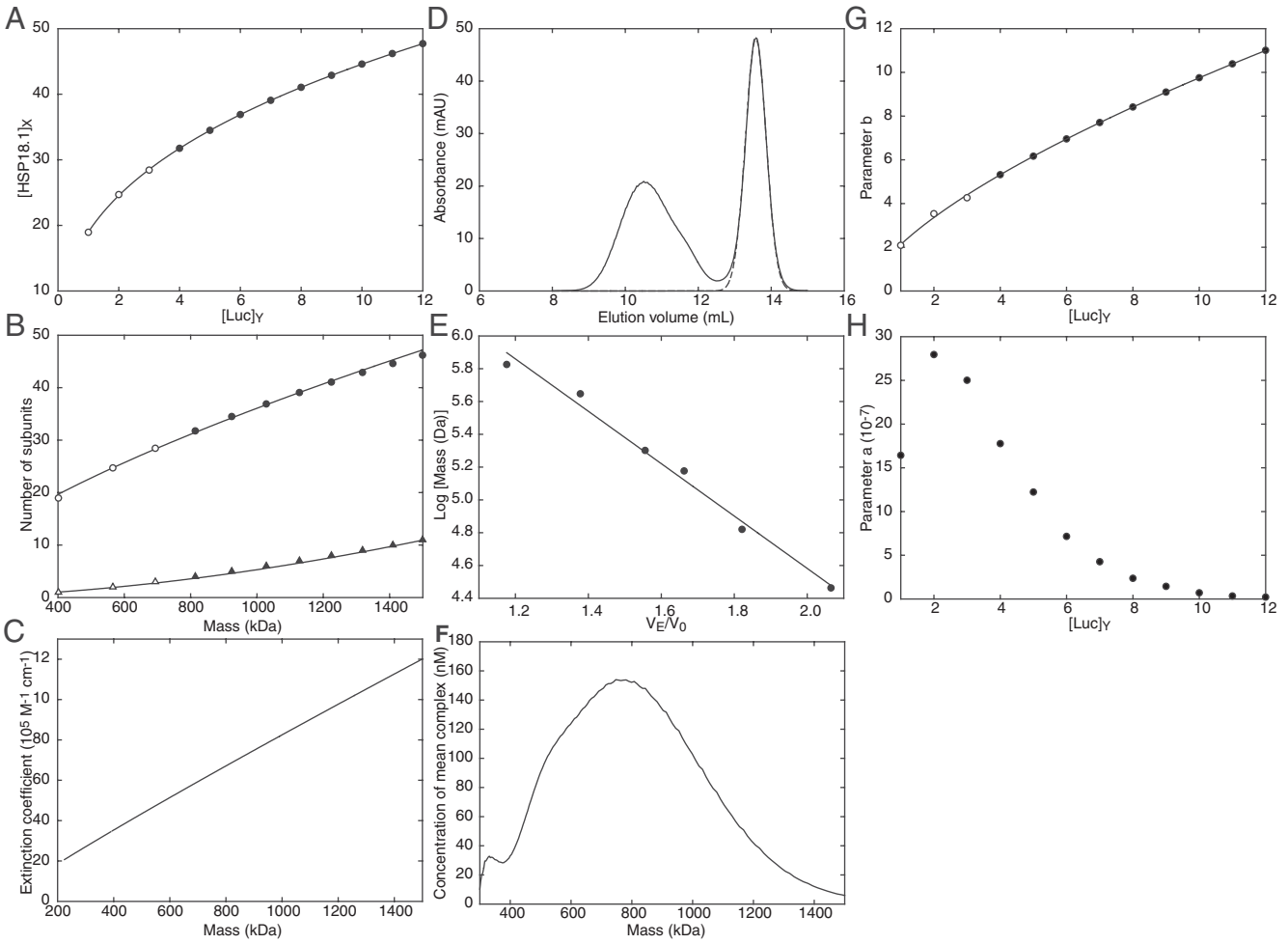

Fig. S10. Extrapolation to obtain full distribution of complexes. To obtain an overall distribution for the complexes formed at a 1 : 1 ratio (Fig. 5*C*) we combined our tandem-MS results with the SEC profile. We derived a relationship between the number of HSP18.1 and Luc subunits from tandem-MS (*A*), and hence the mass dependence of the number of HSP18.1 (circles) and Luc (*Triangles*) subunits (*B*). From this we could estimate the relationship between mass and extinction coefficient (*C*). From the overall SEC profile (*Solid Line*) at a 1 : 1 ratio (*D*), the contribution of dodecamer (*Dashed Line*) was removed. By calibration using standard proteins (*E*), the SEC trace was converted to a mass axis, and, from the relationship in *C*, into a concentration scale (*F*). Gaussian distributions for the different numbers of HSP18.1 at each bound state of Luc, as in Fig. 5*C*, and of form $y = ae^{(-0.5(\frac{x-x_0}{b})^2)}$ were constructed using the trends in mean number of HSP18:1 per Luc (parameter x_0) (*A*); peak width (parameter *b*) (*G*); and intensity (parameter *a*) (*H*), obtained by considering *F* in relation to *B*. In panels *A*, *B*, and *G* empty symbols correspond to the tandem-MS data, and filled symbols to extrapolation. Combining the different Gaussian distributions results in the quantitative three-dimensional distribution map of different complexes (Fig. 5*C*).

3)

$$K_{AV,i} = \sum_{k=1}^{i} K_{ST,k}[P_1]^{i-1}$$

4)

$$\sum_{i=1}^{n} i[P_i] = \sum_{i=1}^{n} iK_{AV,i}[P_1] = \sum_{i=1}^{n} i \sum_{k=1}^{i} K_{ST,k}[P_1]^i$$

5)

$$\chi^2 = \sum_{i}^{N} \frac{\left(\Delta G_i^{\text{exp}} - \Delta G_i^{\text{calc}}\right)^2}{\sigma_i^2}$$